ORIGINAL PAPER

Synchronized nonpharmaceutical interventions for the control of COVID-19

Bing Zhang · Shiwen Liang · Gang Wang · Chi Zhang · Cai Chen · Min Zou · Wei Shen · Haoyu Long · Daihai He · Yuelong Shu · Xiangjun Du

Abstract The world is experiencing an ongoing pandemic of coronavirus disease-2019 (COVID-19), which is caused by severe acute respiratory syndrome coronavirus 2 (SARS-CoV-2). In attempts to control the pandemic, a range of nonpharmaceutical interventions (NPIs) has been implemented worldwide. However, the effect of synchronized NPIs for the control of COVID-19 at temporal and spatial scales has not been well studied. Therefore, a meta-population model that incorporates essential nonlinear processes was constructed to uncover the transmission characteristics of SARS-CoV-2 and then assess the effectiveness of synchronized NPIs on COVID-19 dynamics in China. Regional synchronization of NPIs was observed in China, and it was found that a combination of synchronized NPIs (the travel restrictions, the social distancing and the infection isolation) prevented 93.7% of SARS-CoV-2 infections. The use of synchronized NPIs at the time of the Wuhan lockdown may have prevented as much as 38% of SARS-CoV-2 infections, compared with the unsynchronized scenario. The interconnectivity of the epicenter, the implementation time of synchronized NPIs, and the number of regions considered all affected the performance of synchronized NPIs. The results highlight the importance of using synchronized NPIs in high-risk regions for the control of COVID-19 and shed light on effective strategies for future pandemic responses.

Keywords COVID-19 · Nonpharmaceutical interventions · Synchronization · Social distancing · Infection isolation

Bing Zhang and Shiwen Liang these authors contributed equally to this work.

Supplementary Information The online version contains supplementary material available at https://doi.org/10.1007/s11071-021-06505-0.

B. Zhang · S. Liang · G. Wang · C. Zhang ·
C. Chen · M. Zou · W. Shen · H. Long ·
Y. Shu (✉) · X. Du (✉)
School of Public Health (Shenzhen), Sun Yat-sen University, Guangzhou, China
e-mail: shuylong@mail.sysu.edu.cn

X. Du
e-mail: duxj9@mail.sysu.edu.cn;
xiangjundu@hotmail.com

D. He
Department of Applied Mathematics, Hong Kong Polytechnic University, Hong Kong, China

Y. Shu · X. Du
Key Laboratory of Tropical Disease Control, Ministry of Education, Sun Yat-sen University, Guangzhou, China

1 Introduction

A novel coronavirus, severe acute respiratory syndrome coronavirus 2 (SARS-CoV-2), has caused a global pandemic of coronavirus disease-2019 (COVID-19) [1, 2]. The government of China implemented combinations of nonpharmaceutical interventions (NPIs) to attempt to contain the pandemic [3–5]. These NPIs, which include transportation restrictions, the social distancing of susceptible people, and the use of contact tracing to isolate those infected with SARS-CoV-2, have prevented SARS-CoV-2 from spreading widely and thus enabled effective control of COVID-19 in China [3, 6, 7]. In contrast, a distributed, state-level decision-making process was used in the USA, which resulted in variable enforcement and a pandemic-mitigation response that was highly variable in space and time [8, 9]. It remains an open question whether and how responses to the COVID-19 pandemic should be coordinated [6].

It is well acknowledged that the strength of NPIs and the manner in which they are implemented contribute to their efficacy. At the early stage of the COVID-19 pandemic, NPIs such as restrictions on travel from the epicenter of the coronavirus outbreak played critical roles in delaying the exportation of cases to other regions [6, 10]. However, it is unlikely to fully contain the outbreak solely by nonpharmaceutical interventions in the epicenter, especially as community transmission had already begun in other regions [3]. In today's highly connected world, the spatiotemporally dynamic manner in which infected individuals move between regions can result in the persistence of infection across regions and accelerate the pandemic spread [8]. Thus, the use of coordinated interventions for the control of infection is considered crucial for minimizing the spread of the COVID-19 pandemic and preventing future recurrences [11]. Previous studies have confirmed that appropriate coordination can greatly improve the likelihood of eliminating community transmission [3]. Another study found that uncoordinated government responses to COVID-19 resulted in a substantial cost, due to the movement of people, ideas, and media across borders [12]. These evidences highlighted the spillover effects of joint interventions that can bring benefits for all the involving regions in the presence of coordination.

Understanding the heterogeneity of COVID-19 dynamics in various regions is essential for designing effective strategies to control the disease [13, 14]. Given this heterogeneity, concerns have been raised regarding the optimal way NPIs were implemented, but few studies [3, 13] have fully investigated the effectiveness of regional NPIs in high-risk areas and compared the results of these to the results of the national lockdown strategy. A previous study found that local lockdowns outperformed global lockdown on the far side of the COVID-19 pandemic curve [15]. Given the fact that infections have been shown to disperse spatially between connected population centers in an apparently heterogeneous fashion, it is important that NPI strategies be optimized in a differentiated but coordinated manner to create an overall NPI strategy that is hierarchical and synchronized [3, 16].

Most epidemics are only partially observed, and thus, their dynamics need to be uncovered using ad hoc methods on incomplete data derived from a wide variety of sources and over a wide range of scales. In this context, spatially structured stochastic models are superior to dynamic models of single regions, as the former can capture the regional heterogeneity of disease dynamics, thereby allowing a broader exploration of possible interventions [14, 15]. Previous studies have confirmed the effectiveness of individual NPIs, such as travel restrictions [17], social distancing [7, 18], and isolation of infected individuals [3], in the containment of COVID-19 in China. However, it remains unclear how relatively important these NPIs are for controlling COVID-19 dynamics, and whether they demonstrate synergistic effects. In addition, few studies have explored the effectiveness of synchronized NPIs across regions for the control of COVID-19 in China. Thus, to further border the understanding on the efficiency of NPIs on COVID-19 dynamics, the relative importance and effect of synchronized NPIs for the control of COVID-19 in China were explored in this study, using an informative meta-population model that explicitly incorporates essential components for the transmission of SARS-CoV-2.

2 Materials and methods

2.1 Epidemiological and demographic data

Daily new confirmed COVID-19 cases were obtained from the reports published by the Health Committees of 31 provincial-level administrative units (Fig. 1).

Data from January 16 to February 12, 2020 were used, to avoid complications due to the altered case definition that was implemented after February 12, 2020 (such that only clinically diagnosed cases of COVID-19 were recorded). Population data from 2018 were obtained from the Ministry of Civil Affairs of the People's Republic of China (http://xzqh.mca.gov.cn/map).

2.2 Human mobility data

Daily human mobility data during the study period were collected from the Baidu Qianxi platform (https://qianxi.baidu.com/2020/) and then adjusted according to the population movement statistics published by the Ministry of Transport of the People's Republic of China (http://www.mot.gov.cn). Data for the population movement between 343 cities were extracted (Fig. S1). For simplicity, mean human mobility between regions before and after January 23, 2020, which was the date that public transportation to and from Wuhan was prohibited, was calculated and used in this study. A directed mobility network was constructed, with nodes as cities and edges representing population movement between cities. The interconnectivity of a city was defined as the scaled degree centrality score of the city in the network, which was calculated using the degree function in the R package *sna* [19, 20] (Fig. S2).

Internal mobility (IM) data within cities were also gathered from the Baidu Qianxi Platform. The results from contact surveys in Wuhan and Shanghai showed that the reduction in IM can be used as a proxy for the change in the contact rate [18] and thus used as a measure of the strength of social distancing in the present study. Given the regional heterogeneity of IM across cities, the IM was standardized for each region ($i \in (1, 2, \ldots, n)$), as follows:

$$\mathrm{SIM}_i(t) = \begin{cases} 1, & \text{January } 16 \leq t < \text{January } 24 \\ \dfrac{\overline{IM_{i,\text{intervention}}}}{\overline{IM_{i,\text{baseline}}}}, & \text{January } 24 \leq t \leq \text{February } 12 \end{cases}$$

(1)

where $\mathrm{SIM}_i(t)$ is the standardized IM. The average IM for the region i in the baseline period (January 16–January 23) and that in the intervention period (January 24–February 12) were defined as $\overline{IM_{i,\text{baseline}}}$ and $\overline{IM_{i,\text{intervention}}}$, respectively. The distribution of SIM for each province/municipality after the Wuhan shutdown is shown in Fig. S3.
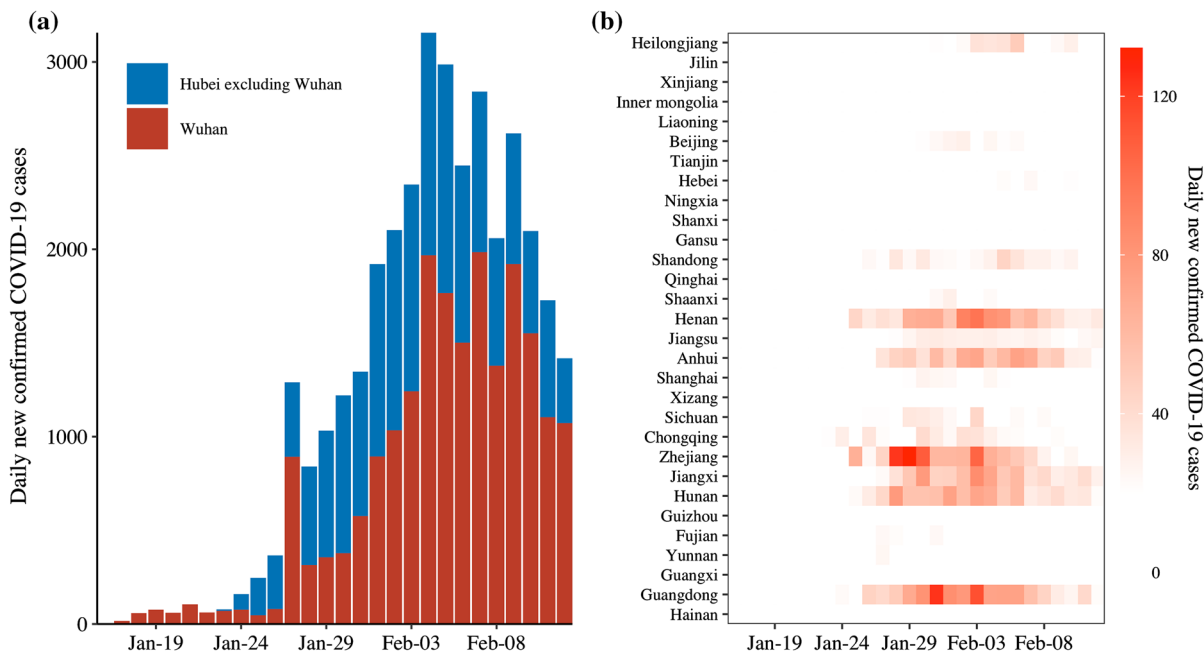

Fig. 1 Dynamic pattern of coronavirus disease-2019 (COVID-19) cases in China from January 24 to February 12, 2020. **a** Histogram of time series of daily numbers of new COVID-19 cases in Hubei Province, China (blue and red represent regions outside and inside Wuhan, respectively). **b** Heatmap of the daily numbers of COVID-19 cases outside Hubei Province

2.3 Meta-population compartment model

A meta-population model for Hubei Province (the Hubei model) was built by integrating regional models of population movement with region-specific and shared parameters [14, 21, 22]. For each region, a $SEI_qI_hI_uR$ model was constructed (Fig. 2), which compartmentalizes a population into categories of susceptible (S) individuals, exposed (E) individuals, infected individuals who are untraceable (IU; silent transmitters), infected individuals who have been isolated (quarantined; IQ), infected individuals who have escaped quarantine (IH), and recovered individuals (R). For region i, the model was formulated as follows:
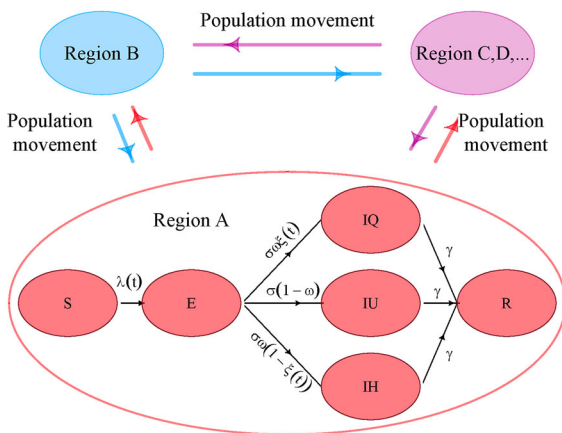

Fig. 2 Model structure of the meta-population Susceptible–Exposed–Infected (untraceable)–Infected (quarantined)–Infected (escaped quarantine)–Recovered model. The population in each region was divided into six compartments: susceptible individuals (S), exposed individuals (E), infected individuals that cannot be traced (IU; silent transmitters), infected individuals who are quarantined (isolated; IQ), infected individuals that escape quarantine (IH), and recovered individuals (R). Regional dynamics were then coupled with population movements. The key model parameters are listed in Table 1
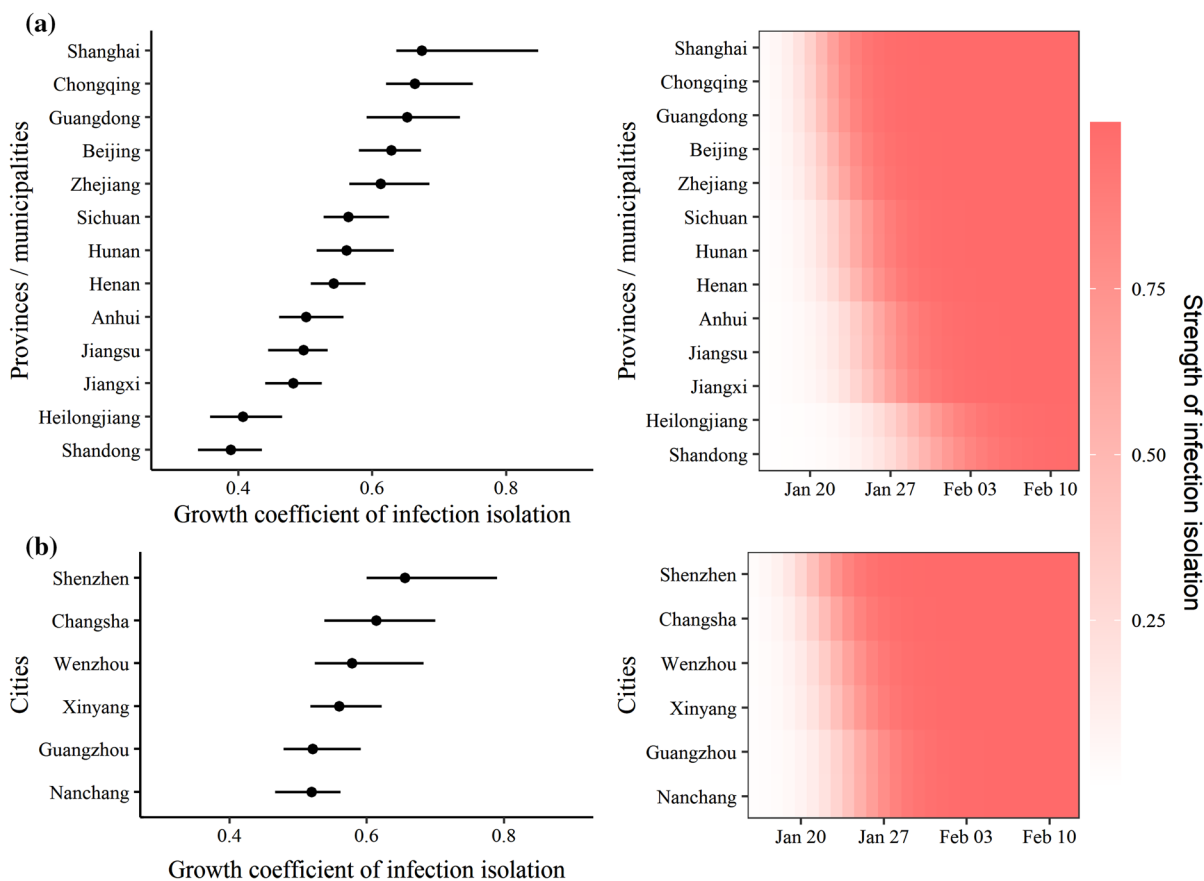
$$\begin{cases} \dfrac{dS_i}{dt} = -\lambda_i(t)S_i \\ \dfrac{dE_i}{dt} = \lambda_i(t)S_i - \sigma E_i \\ \dfrac{dIH_i}{dt} = E_i(1-\xi_i(t))\omega\sigma - \gamma IH_i \\ \dfrac{dIU_i}{dt} = E_i(1-\omega)\sigma - \gamma IU_i \\ \dfrac{dIQ_i}{dt} = E_i\xi_i(t)\omega\sigma - \gamma IQ_i \\ \dfrac{dR_i}{dt} = \gamma(IQ_i + IU_i + IH_i) \\ N_i = S_i + E_i + IH_i + IQ_i + IU_i + R_i \end{cases} \quad (2)$$

where $1/\sigma$ and $1/\gamma$ are the incubation period and infectious period, respectively; ω is the maximum traceable rate of SARS-CoV-2 infections; and $\xi_i(t)$ is the strength of isolation, which represents the time-varying proportion of isolated infections, and is formulated using a sigmoid function with the growth coefficient ξ_i, the covariate t, and the intercept ξ_0:

$$\xi_i(t) = 1/\left(e^{-(\xi_i*t+\log(\xi_0))} + 1\right) \quad (3)$$

Given the difference between the dynamic patterns in Wuhan and non-Wuhan cities in Hubei Province, two distinct parameters, ξ_w and ξ_e, are used to represent the different growth coefficients of the strength of infection isolation interventions in Wuhan and in these other cities.

All of the susceptible individuals in the region i have the infection risk $\lambda_i(t)$, which is formulated as the following equation:

$$\lambda_i(t) = \beta_i(t)\frac{\kappa IH_i + IU_i + \sum_{i\neq j}\left(-\frac{IU_i+\kappa IH_i}{N_i-IQ_i}F_{i,j} + \frac{IU_j+\kappa IH_j}{N_j-IQ_j}F_{j,i}\right)}{N_i - IQ_i} \quad (4)$$

where κ is the relative transmission rate of IH compared to IU; $F_{i,j}$ is the human movement from region i to region j; and $\beta_i(t)$ is the time-varying transmission rate, which is formulated from the basic contact rate during the baseline period (c_0), the transmission probability per contact (β_0), and SIM. To simplify the model structure, only infectors (IU_j and IH_j in Eq. (4)) are specifically considered in the human movement, and the population size is assumed to be constant [22, 23].

In each region at the start of the pandemic, the basic reproduction number R_0 is the largest eigenvalue of the next-generation matrix [24]. Let $X = (E, IU, IH)$

Fig. 3 Estimations of the growth coefficient (left) and strength (right) of infection isolation at provincial (**a**) and city levels (**b**). Only provinces with greater than 300 accumulated cases and cities with greater than 200 accumulated cases were selected. The median value for the growth coefficient and its 95% confidence intervals are depicted in the left panel. The heatmap in the right panel represents the projected strength of infection isolation for each target region

and $Y = (S, R)$. Then, matrix F, which defines the rate of new infections in different compartments, is as follows:

$$F = \begin{pmatrix} \dfrac{\beta_0 cS(\text{IU} + \kappa \text{IH})}{N} \\ 0 \\ 0 \end{pmatrix} \tag{5}$$

Another matrix (V), which defines the rate of transfer of infections from one compartment to another, can be written as follows:

$$V = \begin{pmatrix} \sigma E \\ \gamma \text{IU} - (1-\omega)\sigma E \\ \gamma \text{IH} - \omega \xi_t \sigma E \end{pmatrix} \tag{6}$$

Finally, we have:

$$F = \begin{pmatrix} 0 & \beta_0 c & \kappa \beta_0 c \\ 0 & 0 & 0 \\ 0 & 0 & 0 \end{pmatrix} \quad \text{and}$$

$$V^{-1} = \begin{pmatrix} \dfrac{1}{\sigma} & 0 & 0 \\ \dfrac{1-\omega}{\gamma} & \dfrac{1}{\gamma} & 0 \\ \dfrac{\omega(1-\xi_t)}{\gamma} & 0 & \dfrac{1}{\gamma} \end{pmatrix}$$

The next-generation matrix is $K = FV^{-1} =$

$$\begin{pmatrix} \dfrac{(1-\omega)\beta_0 c + \omega\kappa(1-\xi_t)\beta_0 c}{\gamma} & \dfrac{\beta_0 c}{\gamma} & \dfrac{\kappa\beta_0 c}{\gamma} \\ 0 & 0 & 0 \\ 0 & 0 & 0 \end{pmatrix}.$$
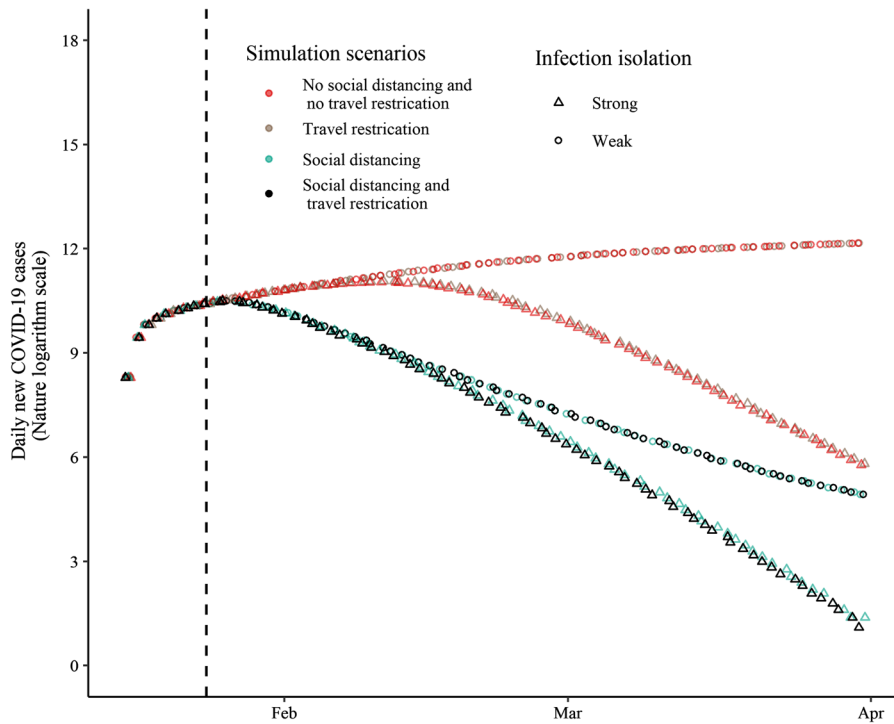
Thus, R_0 is computed as:

Fig. 4 Effects of synchronized nonpharmaceutical interventions (NPIs) on the coronavirus disease-2019 pandemic in China in different scenarios. Four scenarios were tested with two strengths of infection isolation (low and high): no social distancing and no travel restriction measures (red), travel restriction measures only (gray), social distancing measures only (cyan), and social distancing and travel restriction measures (black). Simulations were run based on the national meta-population model. All of the NPIs were implemented after the Wuhan lockdown (dashed line). High-strength infection isolation after the Wuhan lockdown (triangle) was represented by growth coefficients of 0.25 and 0.53 for Wuhan and other regions, respectively (Table 1). Low-strength infection isolation (circle) after the Wuhan lockdown was represented by no change in the strength of infection isolation, which remained at 0.01 and 0.27 in Wuhan and other regions, respectively (Fig. S6)

$$R_0 = \frac{(1 - \omega)\beta_0 c_0 + \omega\kappa\beta_0 c_0}{\gamma} \quad (7)$$

Thus, the force of infection $\lambda_i(t)$ can be reformulated as follows:

$$\lambda_i(t) = \text{SIM}_i(t)\frac{R_0\gamma}{1 - \omega + \omega\kappa}\frac{\kappa IH_i + IU_i + \sum_{i \neq j}\left(-\frac{IU_i + \kappa IH_i}{N_i - IQ_i}F_{i,j} + \frac{IU_j + \kappa IH_j}{N_j - IQ_j}F_{j,i}\right)}{N_i - IQ_i} \quad (8)$$

2.4 Observation process and parameter estimation

In the observation model, the observed number of daily confirmed COVID-19 cases $C_i(t)$ is measured as a normal distribution to allow for over-dispersion of the case counts [25]:

$$C_i(t)|Y_i(t) \sim rnorm(Y_i(t), \varrho Y_i(t)) \quad (9)$$

where ϱ is the reporting over-dispersion; and $Y_i(t)$ represents the number of people moving from class IQ_i to class R_i in region i at time t

Parameters are estimated using the sequential Monte Carlo method in the R package *pomp* [26]. The likelihood function used in this study [25] is formulated as:

$$L_i(t) = pnorm(C_i(t) + 0.5, Y_i(t), \varrho Y_i(t)) \\ - pnrom(C_i(t) - 0.5, Y_i(t), \varrho Y_i(t)) \quad (10)$$

The maximum likelihood estimation of target parameters and its confidence interval (CI) are obtained from the Monte Carlo adjusted profile algorithm [27]. For $C_i(t) = 0$, we replace $C_i(t) - 0.5$ by $-\infty$.

2.5 Model validation

As the study period was short (29 points for each region), the effective identification of the target parameters was of great importance. To test the effectiveness of the inference framework, parameters were estimated based on synthesized data generated from the Hubei model (comprising 17 cities, including Wuhan) and predefined parameters (Table S1). Two scenarios were tested: one scenario had the same strength of infection isolation in Wuhan (ξ_w) and in other cities (ξ_e), i.e., $\xi_e = \xi_w$, and the second scenario had different strengths of infection isolation in Wuhan compared to other cities, i.e., $\xi_e \neq \xi_w$ (Table S1). The detailed procedure used for the model validation is as follows:

1. Predefinition of the parameters (Table S1). The initial states for each city were obtained from the initial state generated by the maximum likelihood estimation in the Hubei model;
2. Based on the predefined parameters (Table S1) and the initial states, median values at each time point were calculated from the synthesized data generated by 100 simulations based on the Hubei model.
3. Key parameters were re-estimated using the inference framework based on the synthesized data, and the re-estimated parameters were compared to the predefined values.

## 2.6 Spatial and temporal synchronization

A meta-population model incorporating 343 cities in China was used for spatial and temporal synchronization, and simulations were run for the period from January 16 to March 31, 2020. To simulate a realistic scenario, the parameters and initial conditions for the selected epicenter and its 16 most highly connected cities were based on values from the Hubei model (comprising Wuhan and 16 non-Wuhan cities in Hubei Province). We assumed that there were no infections in other cities at the beginning of the simulation. The hypothetical epicenter could be one of the 31 capital cities in China. Synchronization of NPIs was defined as selected cities (n_i) implementing NPIs simultaneously at time t_i, while the remaining cities implemented NPIs at a random time between t_i and $t_i + 7$. The implementation of travel restrictions (population

movement between regions) and social distancing (measured as SIM) was represented by using the mobility data after the Wuhan lockdown (Fig. S3). To represent the strength of infection isolation, the strength in the city i was first set as constant between January 23 and t_i and then allowed to increase after the implementation of NPIs: the growth coefficients of this increase in the epicenter and other cities were set using the estimated growth coefficients for Wuhan and non-Wuhan cities, respectively, in the Hubei model. The effect of synchronized NPIs was defined as the proportion of infections that were averted compared to the unsynchronized scenario. Linear regression was performed using the *lm* function in R software to determine the relationship between the effect of synchronized NPIs and the interconnectivity of a specific city (as a hypothetical epicenter).

3 Results

3.1 Hubei model

A meta-population model for cities in Hubei Province was established by incorporating different categories of infected individuals: IU, IQ, and IH. The model also specifically incorporates the social distancing in the transmission rate and strength of infection isolation (Fig. 2). The inference framework was tested on synthesized datasets, and it was found that all of the parameters could be correctly re-estimated, irrespective of the differences between the strength of infection isolation in Wuhan and other cities in Hubei Province (Table S1 and Fig. S4; details in Materials and Methods). The meta-population model captured the dynamics of COVID-19 across cities in Hubei Province (Fig. S5), and the maximum likelihood estimations for the key parameters are shown in Table 1. The maximum proportion of infections that could be traced was estimated as 0.93 (95% CI 0.84–0.96), suggesting that 7% of SARS-CoV-2 infections were due to silent transmitters, who are difficult to trace. Compared to IU, the relative transmission rate of IH was at 1.22 (95% CI 0.65–1.65). The growth coefficient for the strength of infection isolation was larger in non-Wuhan cities than in Wuhan itself, as shown by the respective values of 0.53 (95% CI 0.45–0.56) and 0.25 (95% CI 0.22–0.27) (Table 1). It was estimated that the strength

(a) Wuhan / Chengdu / Beijing

(b)

(c)
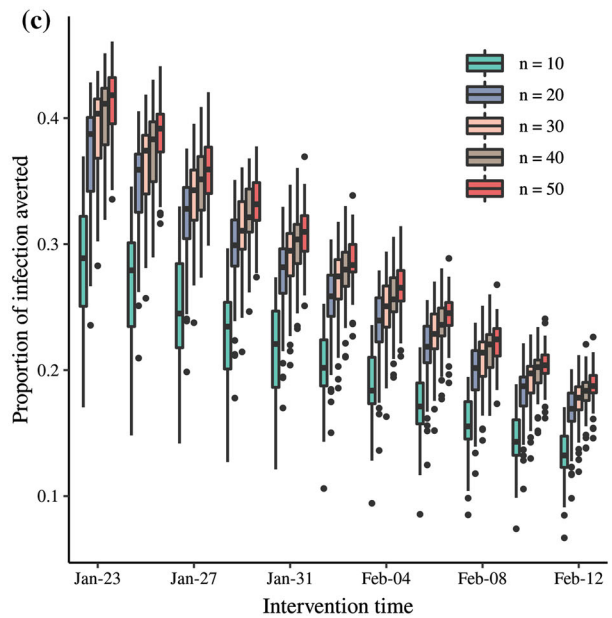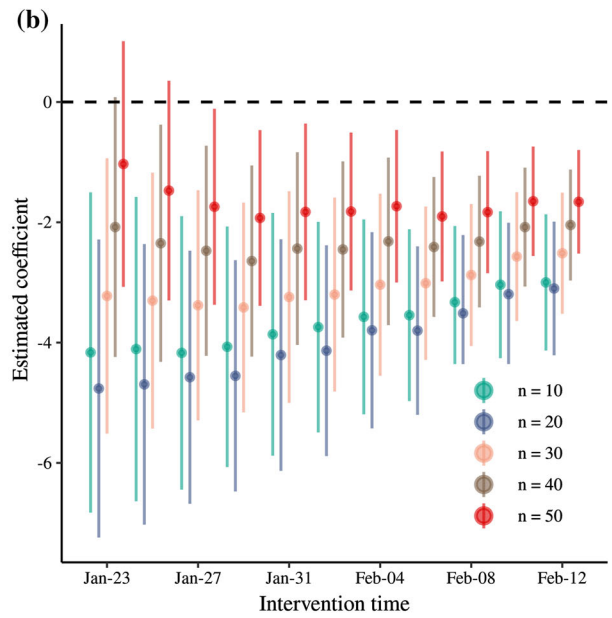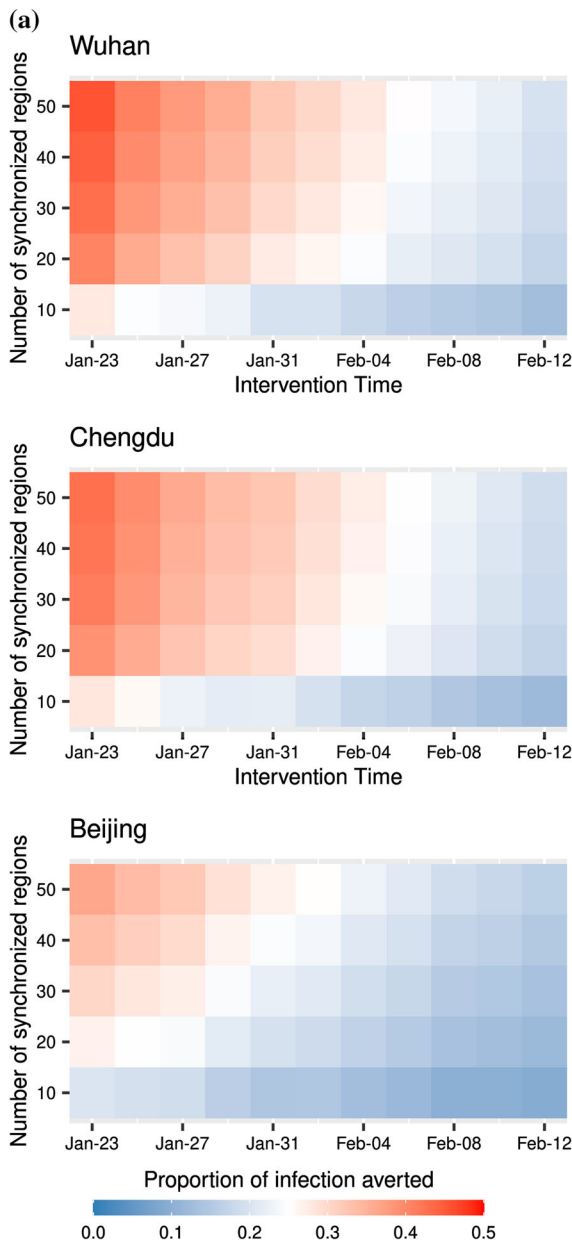
of infection isolation for non-Wuhan cities in Hubei Province increased to 0.95 on February 1 and then remained almost constant (Fig. S6). However, the strength of infection isolation in Wuhan was maintained at a low level (< 0.1) before February 1, and then increased to 0.59 on February 12 (Fig. S6).

3.2 Synchronization of interventions

There was a synchronized decrease in the population movement between regions and in the internal mobility within cities after the Wuhan lockdown (Fig. S3). The mean decrease in within-city mobility was 49.6% (95% CI 27.5–70.0%) in the intervention period (January 24–February 12) compared to the baseline period (January 16–January 23). On average, 60.2% of

◀**Fig. 5** Effect of synchronized nonpharmaceutical interventions (NPIs) on the control of coronavirus disease-2019 (COVID-19) in China. **a** Effect of synchronized NPIs with the hypothetical epicenter located in Wuhan (medium interconnectivity), Chengdu (low interconnectivity), and Beijing (high interconnectivity). Interconnectivity was defined as the scaled degree-centrality score in the weighted network, with nodes as cities and edges representing population movement between cities. The effect of synchronized NPIs was measured as the proportion of infections that were averted compared to the unsynchronized situation (see Materials and Methods for more details). Model simulations were performed with different intervention times (from January 23 to February 12, with an interval of 2 days) and different spatial coverages (the number of coordinated cities ranged from 10 to 50, with an interval of 10) from January 16 to March 31. Parameters from the Hubei model were used for the initial states of an epicenter and the 16 cities with which it was most connected. In other regions, it was assumed there were no infections on January 16. **b** Relationship between the effect of synchronized NPIs and the interconnectivity of a hypothetical epicenter. The *y*-axis shows the estimated coefficient of the linear regression between the effect of synchronized NPIs and the city interconnectivity of the selected epicenter. **c** Effect of synchronized NPIs with different intervention times. The color boxplot represents various spatial coverages of the synchronized NPIs. The hypothetical epicenter in each simulation is one of 31 capital cities in China

the cities showed a noticeable decrease ($> 50\%$) in the population movement between regions from January 24 to February 12. To determine whether there was regional synchronization in the strength of infection isolation, a region-specific model was constructed by adding a target region into the Hubei model. Only provinces with greater than 300 accumulated cases and cities with greater than 200 accumulated cases were used for robust estimations (Fig. 1). Obvious regional synchronization was observed in the strength

of infection isolation outside Hubei Province (Fig. 3). The growth coefficient for the strength of infection isolation was the highest in Shanghai among the selected regions, followed by those in Chongqing, Guangdong, and Beijing (Fig. 3a, left). All of the selected regions had a high strength of infection isolation close to 1 on February 12 (Fig. 3a, right). At the city level, the estimated growth coefficient for the strength of infection isolation in six selected cities was greater than 0.5, with the highest value observed in Shenzhen (Fig. 3b).

3.3 Effect of synchronized NPIs at the national scale

To evaluate the effect of synchronized NPIs at the national scale, a national model was built using the same model structure and by incorporating the mobility data of 343 cities (see Materials and Methods for more details). Two scenarios of the strength of infection isolation were tested: low-strength infection isolation, i.e., no change in the strength of infection isolation after the Wuhan lockdown and high-strength infection isolation (the growth coefficients of 0.25 for Wuhan and 0.53 for other regions, Fig. S6). The implementation of only travel restrictions in the low- and high-strength infection isolation scenarios had a limited effect on SARS-CoV-2 infections (Fig. 4). However, the implementation of only social distancing measures suppressed 93.2% and 73.4% of SARS-CoV-2 infections in the low- and high-strength infection isolation scenarios, respectively. This shows that social distancing measures alone could contain the COVID-19 pandemic in China; however, more

Table 1 Parameter estimations in the Hubei model

Parameter	Median (95% confidence intervals)
Latency period (σ, day^{-1})	6.17 (4.35 – 8.78)
Infectious period (γ, day^{-1})	5.08 (4.09 – 6.03)
Basic reproduction number (R_0)	1.71 (1.27 – 2.13)
Maximum traceable rate of SARS-CoV-2 infection (ω)	0.93 (0.84 – 0.96)
Relative transmission rate of IH compared with IU (κ)	1.22 (0.65 – 1.65)
Intercept for the strength of infection isolation (ξ_0)	0.0003 (0.0001 – 0.0006)
Growth coefficient of the strength of infection isolation in Wuhan (ξ_w)	0.25 (0.22 – 0.27)
Growth coefficient of the strength of infection isolation in non-Wuhan cities in Hubei (ξ_e)	0.53 (0.45 – 0.56)

unrecorded infections were averted when strict infection-isolation interventions were implemented simultaneously (Fig. S7). The enhanced infection isolation interventions have reduced 76.0% of the infections and prevented 93.7% of the infections if combined with the social distancing and travel restriction measures (Fig. 4).

3.4 Effect of synchronized NPIs at temporal and spatial scales

A deeper understanding of how synchronized NPIs affect COVID-19 dynamics in China was gained by evaluating the effect of combined interventions with various implementation time and region coverage, and of various epicenter interconnectivities, based on the national model (see Materials and Methods for more details). The results show that the benefits of NPI synchronization increased as the number of cities involved increased. With Wuhan as the epicenter (Fig. 5a, top panel), a comparison of the unsynchronized situation (see Materials and Methods for details) with the synchronized one (in Wuhan and in the ten cities with which it is most connected) shows that synchronized NPIs decreased SARS-CoV-2 infections by 23.9% (95% CI 15.6 – 31.2%) when the NPIs began on January 23, and decreased SARS-CoV-2 infections by 38.0% (95% CI 32.7 – 42.9%) when the number of regions applying synchronized NPIs reached 50. With Chengdu (a city with less interconnectivity than Wuhan) as the epicenter (Fig. 5a, middle panel), a comparison of the unsynchronized NPIs with synchronized NPIs (in Chengdu and in the 20 and 50 cities with which it is most connected) gave comparable results, with SARS-CoV-2 infection decreases of 38.9% and 42.9%, respectively. However, if the epicenter was located in a region that is highly connected to other regions, such as Beijing (Fig. 5a, lower panel), similar performances were achieved only from the earlier implementation of synchronized NPIs in greater numbers of cities. Linear regression analysis revealed that the interconnectivity of an epicenter was negatively correlated with the effect of synchronized NPIs (Fig. 5b), and this phenomenon was more obvious when synchronized NPIs were applied in fewer cities. In addition, the proportion of infections averted by the synchronized NPIs decreased with the delayed implementation time, irrespective of whether the epicenter was located in the highly

interconnected region, and the effect could not be compensated by increasing the number of synchronized regions (Fig. 5c).

4 Discussion

We developed a meta-population model that explicitly incorporates processes that are essential for the transmission of SARS-CoV-2, and used this model to quantify key parameters for the transmission of SARS-CoV-2 and systematically explore the effect of synchronized NPIs on COVID-19 dynamics in China. We also investigated how the performance of synchronized NPIs was affected by the interconnectivity of an epicenter, the implementation time, and the number of regions that implemented synchronized NPIs.

The analysis of time-series data from a collection of related regions provides opportunities to determine the complex and nonlinear dynamics of a realistic system [21]. To effectively identify the key epidemiological parameters in a short time series, a meta-population model that considered regional heterogeneity in the strength of NPIs was constructed. This model was validated using the synthesized datasets, which guaranteed the feasibility and validity of its modeling and inference framework, even in situations where there was regional heterogeneity in the value of a key parameter. Although several parameters, such as the infectious period and latency period, can be predetermined based on current knowledge, we estimated these using our model and inference framework. The consistencies between the estimated values and the results from an epidemiological study [28] further validate that the structure of our model and algorithm are valid for parameter estimations.

Based on model estimations, the value of R_0 was found to be 1.71, which is lower than the values in previous studies [10, 29]. In the present study, we did not consider the effects of NPIs on the transmission probability per contact. However, other self-prevention measures, such as wearing a mask, may be implemented together with social distancing measures. Thus, the value of R_0 may vary according to the decrease in the transmission probability per contact. It has also been proposed that asymptomatic patients play a significant role in the ongoing pandemic [10, 30, 31], and we found that nearly 7% of infections

were the 'silent spreaders.' This proportion was smaller compared with the proportion of infections due to asymptomatic individuals estimated in other studies [32], which indicated that contact tracing and testing measures in China were an effective infection isolation policy that isolated both the symptomatic and asymptomatic infections. In addition, we found that the transmission rate for symptomatic patients relative to that of these silent spreaders was 1.22, which reveals the importance of identifying and isolating asymptomatic patients to prevent the onward transmission of SARS-CoV-2.

The movement of infected individuals between regions and the heterogeneity of transmission dynamics can result in disease persistence for a long time [8]. Thus, it is critical to optimize intervention strategies in a coordinated manner to best mitigate the COVID-19 pandemic. In the present study, we examined the effect of the synchronization of NPIs in various regions of China, where these NPIs were travel restrictions, social distancing measures, and infection isolation. Our model simulations revealed that the separate implementation of social distancing and infection isolation measures decreased SARS-CoV-2 infections by 93.2% and 76.0%, respectively, and by 93.7% when combined together with travel restrictions. In addition, the strength of NPIs and the manner in which they are implemented contribute to their efficacy. Given that pathogens can spread rapidly between regions during a pandemic, the inter-regional coordination of control measures is critical [8, 11]. We found that the synchronized implementation of NPIs in regions with high interconnectivity affords greater benefits than the use of non-synchronized NPIs, even in the late stages of a pandemic (Fig. 5). We also determined that the interconnectivity of an epicenter, the start time of implementation of NPIs, and the number of regions that implement synchronized NPIs affect the ability of synchronized NPIs to control COVID-19. These quantitative analyses will be useful to enable precise control of COVID-19 in regions where the pandemic is ongoing and there is regional heterogeneity in SARS-CoV-2 transmission.

Several limitations to this study should be acknowledged. First, the compartmental model used in the present study does not capture the individual-level heterogeneity, which may be an important factor in person-to-person contact-driven transmission [12]. Second, recent work has suggested that both pre-symptomatic and asymptomatic individuals may contribute considerably to SARS-CoV-2 transmission [31, 32]. In the present study, we included asymptomatic transmission, but we did not explicitly model pre-symptomatic transmission. Third, we measured the effectiveness of synchronized NPIs on COVID-19 dynamics based on simplified assumptions, which will not apply in real-life scenarios. Future research should be directed toward a better understanding of COVID-19 dynamics, and optimal strategies should be explored for controlling the transmission of SARS-CoV-2 in real-life settings. Finally, we used the reduction in human intercity mobility recorded on the Baidu platform as a proxy for the change in the contact rate in the $SEI_qI_hI_uR$ model [12]. Thus, whether this model can be directly used in other locations should be carefully investigated. Alternatively, linear or nonlinear formulations that use Google mobility data to represent changes in the contact rate may prove effective [9]. In addition, given the regional heterogeneity in contact patterns and environmental conditions [33, 34], the model parameters should be re-estimated to facilitate a re-evaluation of the effectiveness of synchronized NPIs for the control of COVID-19 [35].

Data availability https://github.com/Spatial-R/SpatEPI_COVID.Code availability https://github.com/Spatial-R/SpatEPI_COVID.

Declaration

References

1. Zhu, N., Zhang, D., Wang, W., Li, X., Yang, B., Song, J., et al.: A novel coronavirus from patients with pneumonia in China, 2019. N Engl J Med. **382**, 727–733 (2020)

2. Han, C., Li, M., Haihambo, N., Babuna, P., Liu, Q., Zhao, X., et al.: Mechanisms of recurrent outbreak of COVID-19: a model-based study. Nonlinear Dyn. (2021). https://doi.org/10.1007/s11071-021-06371-w

3. Lai, S., Ruktanonchai, N.W., Zhou, L., Prosper, O., Luo, W., Floyd, J.R., et al.: Effect of non-pharmaceutical interventions to contain COVID-19 in China. Nature **585**, 410–413 (2020)

4. Maier, B.F., Brockmann, D.: Effective containment explains subexponential growth in recent confirmed COVID-19 cases in China. Science **368**, 742–746 (2020)

5. Wu, K., Darcet, D., Wang, Q., Sornette, D.: Generalized logistic growth modeling of the COVID-19 outbreak: comparing the dynamics in the 29 provinces in China and in the rest of the world. Nonlinear Dyn. **101**, 1561–1581 (2020)

6. Chinazzi, M., Davis, J.T., Ajelli, M., Gioannini, C., Litvinova, M., Merler, S., et al.: The effect of travel restrictions on the spread of the 2019 novel coronavirus (COVID-19) outbreak. Science **368**, 395–400 (2020)

7. Prem, K., Liu, Y., Russell, T.W., Kucharski, A.J., Eggo, R.M., Davies, N., et al.: The effect of control strategies to reduce social mixing on outcomes of the COVID-19 epidemic in Wuhan, China: a modelling study. Lancet Public Health. **5**, e261–e270 (2020)

8. Kortessis, N., Simon, M.W., Barfield, M., Glass, G.E., Singer, B.H., Holt, R.D.: The interplay of movement and spatiotemporal variation in transmission degrades pandemic control. Proc. Natl. Acad. Sci. U S A **117**, 30104–30106 (2020)

9. Badr, H.S., Du, H., Marshall, M., Dong, E., Squire, M.M., Gardner, L.M.: Association between mobility patterns and COVID-19 transmission in the USA: a mathematical modelling study. Lancet Infect. Dis. **20**, 1247–1254 (2020)

10. Wells, C.R., Sah, P., Moghadas, S.M., Pandey, A., Shoukat, A., Wang, Y., et al.: Impact of international travel and border control measures on the global spread of the novel 2019 coronavirus outbreak. Proc. Natl. Acad. Sci. U S A. **117**, 7504–7509 (2020)

11. Ruktanonchai, N.W., Floyd, J.R., Lai, S., Ruktanonchai, C.W., Sadilek, A., Rente-Lourenco, P., et al.: Assessing the impact of coordinated COVID-19 exit strategies across Europe. Science **369**, 1465–1470 (2020)

12. Holtz, D., Zhao, M., Benzell, S.G., Cao, C.Y., Rahimian, M.A., Yang, J., et al.: Interdependence and the cost of uncoordinated responses to COVID-19. Proc. Natl. Acad. Sci. U S A. **117**, 19837–19843 (2020)

13. Della Rossa, F., Salzano, D., Di Meglio, A., De Lellis, F., Coraggio, M., Calabrese, C., et al.: A network model of Italy shows that intermittent regional strategies can alleviate the COVID-19 epidemic. Nat. Commun. **11**, 5106 (2020)

14. Quaranta, G., Formica, G., Machado, J.T., Lacarbonara, W., Masri, S.F.: Understanding COVID-19 nonlinear multi-scale dynamic spreading in Italy. Nonlinear Dyn. **101**, 1583–1619 (2020)

15. Karatayev, V.A., Anand, M., Bauch, C.T.: Local lockdowns outperform global lockdown on the far side of the COVID-19 epidemic curve. Proc. Natl. Acad. Sci. U S A. **117**, 24575–24580 (2020)

16. Li, R., Chen, B., Zhang, T., Ren, Z., Song, Y., Xiao, Y., et al.: Global COVID-19 pandemic demands joint interventions for the suppression of future waves. Proc. Natl. Acad. Sci. U S A. **117**, 26151–26157 (2020)

17. Tian, H., Liu, Y., Li, Y., Wu, C.H., Chen, B., Kraemer, M.U.G., et al.: An investigation of transmission control measures during the first 50 days of the COVID-19 epidemic in China. Science **368**, 638–642 (2020)

18. Zhang, J., Litvinova, M., Liang, Y., Wang, Y., Wang, W., Zhao, S., et al.: Changes in contact patterns shape the dynamics of the COVID-19 outbreak in China. Science **368**, 1481–1486 (2020)

19. Newman, M.E.J.: The structure and function of complex networks. SIAM Rev. **45**, 167–256 (2003)

20. Butts, C.T.: Social network analysis with SNA. J. Stat. Softw. **24**, 1–51 (2008)

21. Bretó, C., Ionides, E.L., King, A.A.: Panel data analysis via mechanistic models. J. Am. Stat. Assoc. **115**, 1–21 (2019)

22. Xia, Y., Bjørnstad, O.N., Grenfell, B.T.: Measles metapopulation dynamics: a gravity model for epidemiological coupling and dynamics. Am. Nat. **164**, 267–281 (2004)

23. Ferretti, L., Wymant, C., Kendall, M., Zhao, L., Nurtay, A., Abeler-Dörner, L., et al.: Quantifying SARS-CoV-2 transmission suggests epidemic control with digital contact tracing. Science **368**, eabb6936 (2020)

24. Diekmann, O., Heesterbeek, J.A., Roberts, M.G.: The construction of next-generation matrices for compartmental epidemic models. J. R. Soc. Interface **7**, 873–885 (2010)

25. He, D., Ionides, E.L., King, A.A.: Plug-and-play inference for disease dynamics: measles in large and small populations as a case study. J. R. Soc. Interface **7**, 271–283 (2010)

26. King, A.A., Nguyen, D., Ionides, E.L.: Statistical inference for partially observed Markov processes via the R Package pomp. J. Stat. Softw. **69**, 1–43 (2016)

27. Ionides, E.L., Breto, C., Park, J., Smith, R.A., King, A.A.: Monte Carlo profile confidence intervals for dynamic systems. J. R. Soc. Interface **14**, 20170126 (2017)

28. Li, Q., Guan, X., Wu, P., Wang, X., Zhou, L., Tong, Y., et al.: Early transmission dynamics in Wuhan, China, of novel coronavirus-infected pneumonia. N. Engl. J. Med. **382**, 1199–1207 (2020)

29. Li, R., Pei, S., Chen, B., Song, Y., Zhang, T., Yang, W., et al.: Substantial undocumented infection facilitates the rapid dissemination of novel coronavirus (SARS-CoV-2). Science **368**, 489–493 (2020)

30. Zou, L., Ruan, F., Huang, M., Liang, L., Huang, H., Hong, Z., et al.: SARS-CoV-2 viral load in upper respiratory specimens of infected patients. N. Engl. J. Med. **382**, 1177–1179 (2020)

31. Bai, Y., Yao, L., Wei, T., Tian, F., Jin, D.Y., Chen, L., et al.: Presumed asymptomatic carrier transmission of COVID-19. JAMA **323**, 1406–1407 (2020)

32. Mizumoto, K., Kagaya, K., Zarebski, A., Chowell, G.: Estimating the asymptomatic proportion of coronavirus disease 2019 (COVID-19) cases on board the Diamond

Princess cruise ship, Yokohama, Japan, 2020. Euro Surveill. **25**, 2000180 (2020)

33. Rocklöv, J., Sjödin, H.: High population densities catalyse the spread of COVID-19. J. Travel. Med. **27**, taaa038 (2020)

34. Carleton, T., Cornetet, J., Huybers, P., Meng, K.C., Proctor, J.: Global evidence for ultraviolet radiation decreasing COVID-19 growth rates. Proc. Natl. Acad. Sci. U S A **118**, e2012370118 (2021)

35. Pei, S., Kandula, S., Shaman, J.: Differential effects of intervention timing on COVID-19 spread in the United States. Sci. Adv. **6**, eabd6370 (2020)